ON THE USE OF MOMENTUM AND KINETIC ENERGY TUBES FOR ANALYZING TRANSPORT PHENOMENA IN A SUPERSONIC EJECTOR

Lamberts O.*, Bartosiewicz Y., Chatelain P.
*Author for correspondence
Institute of Mechanics, Materials and Civil Engineering (iMMC),
Université catholique de Louvain (UCL),
Louvain-la-Neuve, 1348,
Belgium,
E-mail: olivier.lamberts@uclouvain.be

ABSTRACT

This work aims at providing novel insights into the entrainment and energy exchange phenomena within a supersonic ejector. To this end, advanced analysis tools based on momentum and energy tubes (Meyers and Meneveau [1]) are extended to the compressible nature of the flow and applied to the transport and mixing phenomena within the ejector. New indicators of mixing are introduced in order to investigate quantitatively transfer between the primary and the secondary streams all along the ejector. It is shown that there is no analogy between the transfer of momentum and the gain in exergy of the secondary stream.

INTRODUCTION

In the current context of growing energy concerns, considerable attention is being paid to the enhancement of the performance of processes in a wide range of areas. Regarding refrigeration systems, supersonic ejectors offer an interesting means to compress a fluid by using low grade energy sources which would be wasted otherwise. Fig. 2 shows the typical layout of an ejector. Devoid of any moving parts, they are passive devices: a motive primary stream entrains the fluid to be compressed in a secondary stream, referred to with the index 1 and 2, respectively. The primary stream, coming from a heat recovery boiler, is driven into the ejector through a primary nozzle. It is accelerated and then choked at the throat of this primary nozzle, and exhausts as a supersonic jet at the exit of the primary nozzle, where it comes into contact with the secondary stream that comes from the evaporator. Depending on the geometry of the ejector and the operating conditions, the secondary stream may also become sonic/supersonic within the ejector. As a compressor, the ejector performance could be evaluated by a characteristic curve giving the entrainment ratio, $\omega = \dot{m}_2/\dot{m}_1$, versus the back pressure, $p(x_b)$. A typical characteristic curve is shown in Fig. 3. For a certain range of values of the back pressure, the entrainment ratio is constant, since both flows are choked within the ejector. The ejector is said to operate in on-design conditions. Beyond a certain critical back pressure, the entrained mass flow rate becomes sensitive to downstream conditions, and the entrainment ratio decreases rapidly until it reaches zero when the back pressure equals a breakdown value. Between the critical and the breakdown back pressures, the ejector is said to operate in off-design conditions. In a refrigeration cycle, the back pressure is the condensation pressure and is then imposed by external conditions.

NOMENCLATURE

e_t	[J/kg]	Specific total exergy
$\overline{\boldsymbol{F}}_K$	[kg/s^3]	Total kinetic energy flux vector field
$\overline{\boldsymbol{F}}_m$	[kg/m/s^2]	Total linear momentum flux vector field
h	[J/kg]	Specific static enthalpy
h_t	[J/kg]	Specific total enthalpy
I_K	[-]	Cumulative transfer of kinetic energy
I_m	[-]	Cumulative transfer of momentum
$\dot{m}$	[kg/s]	Mass flow rate
p	[bar]	Static pressure
p_t	[bar]	Total pressure
s	[J/K/kg]	Specific entropy
T	[K]	Static temperature
T_t	[K]	Total temperature
x	[m]	Horizontal coordinate
x_b	[m]	Horizontal coordinate at the outlet of the ejector
x_{nxp}	[m]	Horizontal coordinate at the nozzle exit position
y	[m]	Vertical coordinate

Special characters

$\boldsymbol{\zeta}$	[-]	Constant unit vector
ξ	[-]	Gain in exergy of the secondary stream
ω	[-]	Entrainment ratio

Subscripts

ref	Reference conditions
0	Reservoir conditions
1	Value associated to the primary stream
2	Value associated to the secondary stream

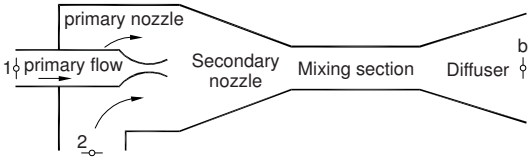

Figure 2. Typical layout of an ejector

Due to a lack of understanding of the complex flow phenomena at play within the ejector, errors in predicting entrainment by 1D models may be significant [2, 3]. For this reason, numer-

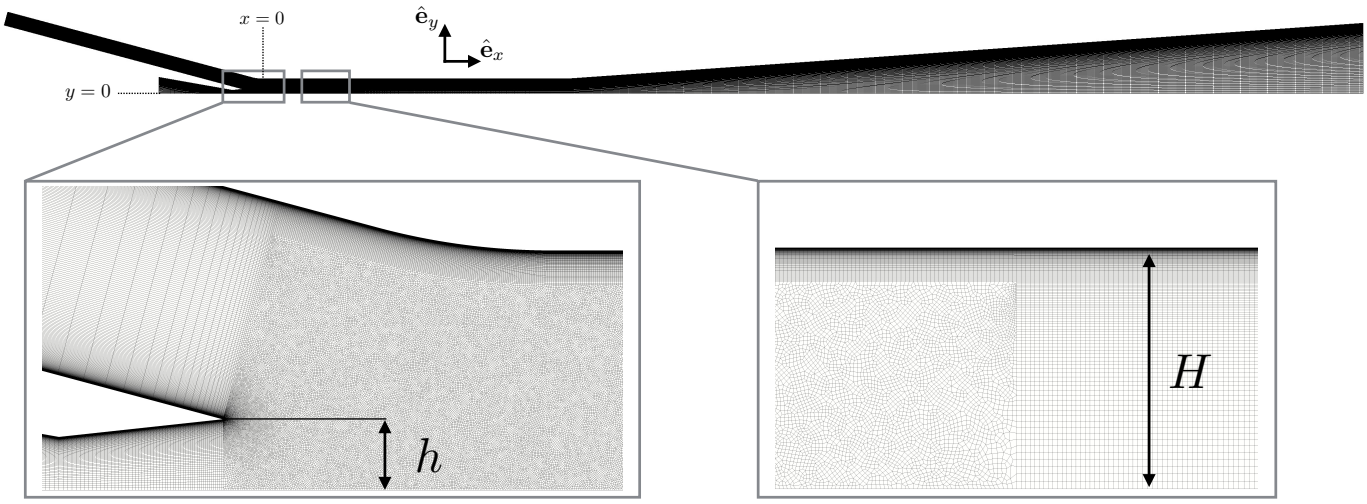

Figure 1. Grid structure of the computational domain for numerical simulations

ical simulations based on CFD have been used in many papers for predicting the behaviour of supersonic ejectors under varying operating conditions and/or geometries. More recently, different studies have investigated the flow structure within the ejector [3–6]. However, the analysis is often limited to iso-contours of Mach number and pressure profiles, which are not really appropriate to assess local mixing and transfer phenomena and their connection with the entrainment ratio. Although the exergy destruction within the ejector is investigated in [6], no distinction is made between the primary and the secondary streams, and no information is given concerning transfers. In the present study, advanced analysis tools based on momentum and energy tubes (Meyers and Meneveau [1]) are extended to the present compressible flow context and applied to the ejector mixing phenomena. New indicators of mixing are introduced in order to investigate quantitatively transfer between the primary and the secondary streams all along the ejector.

NUMERICAL METHOD

Flow solver

The present numerical simulations were produced by means of the open-source software for CFD, OpenFoam 2.3. OpenFoam relies on a Finite Volume method working with either a structured or unstructured discretization. Regardless of the solver, variables are colocated and defined at cell centers, and the governing equations are solved through a segregated approach.

The compressible Reynolds-averaged Navier-Stokes equations are solved by means of an unsteady density-based compressible flow solver that uses an alternative approach to Riemann solvers based on central-upwind schemes of Kurganov and Tadmor [7]. The solver, named *rhoCentralFoam*, is described in details in the original paper of Greenshields et al. [8]. The wall-resolved SST $k-\omega$ turbulence model is used in the present study.

For the selected solver, the continuity equation that provides the density field is solved explicitly while the resolution of the momentum and the energy equations uses an operator-splitting approach: firstly, an explicit predictor equation is solved for the convection of *conserved* variables ($\overline{\rho}\hat{\mathbf{u}}$ and $\overline{\rho}\hat{E}$), then the diffusion of *primitive* variables ($\hat{\mathbf{u}}$ and T) is taken into account through the resolution of an implicit corrector equation. Finally, the equation of state is used to obtain the pressure field. Note that the working fluid is assumed to be a perfect gas. Because *rhoCentralFoam* is an unsteady solver, we consider that the solution achieves a steady state as soon as the relative difference in mass flow rates between the inlet and outlet boundaries remains below 5.10^{-4}.

Geometrical modeling

In the present work, a rectangular supersonic ejector using air as working fluid is analysed. The ejector that has been simulated corresponds to the rectangular ejector of the experimental setup available at UCL and described in details in [9]. The flow within the ejector is simulated numerically as symmetrical. Although Mazzelli et al. [9] showed that 3D simulations performed better than 2D simulations in on- and off-design conditions, the errors for the prediction of the entrainment ratio are comparable in the on-design regime. The present study does not aim at investigating discrepancies between 2D and 3D numerical results but rather focuses on introducing novel post-processing tools in order to shed light on the mixing phenomena. Hence, we can restrict this study to 2D simulations.

The grid structure of the numerical domain is shown in Fig.1. The mesh has been generated via GMSH [10]. It is mainly structured apart from the part that connects both inlets at the primary nozzle exit region and makes the transition to the mixing section. The mesh passes from unstructured to structured at the end of the first quarter of the mixing section. The mesh is also refined in the vertical direction in order to ensure that the centre of the cell adjacent to the wall is always at $y^+ \approx 1$. In total, the mesh is composed of approximately 350,000 hexahedra. The origin is located on the plane of symmetry of the ejector, at the entry of the mixing duct.

The grid independence has been checked through the comparison of the profile of the Mach number on the axis of the ejector for the mesh described here above and a refined mesh. The finer mesh was obtained by refining the normal one only in the axial direction and solely in the structured zones, yielding a mesh of approximately 535,000 cells. The maximum difference between both profiles was found to be less than 2.5%.

Boundary conditions

The flow being subsonic at the primary and secondary inlets, total temperatures (T_{01} and T_{02}) and pressures (p_{01} and p_{02}) are then imposed as boundary conditions. The values of the primary total pressure that has been used in this study is $p_{01} = 3.5\,[\text{bar}]$ and corresponds to an overexpanded motive flow at the primary nozzle exit plane. As the secondary stream is sucked from the atmosphere, its total pressure is very close to $1\,[\text{bar}]$ for all cases. For k and ω at inlets, the value of the turbulence intensity and a specific mixing length were prescribed. At the outlet, the only variable that is imposed is the static pressure ($p(x_b)$). Walls are all assumed adiabatic.

Verification and validation

The numerical results are validated with experimental data in two different ways. In a first approach, one characteristic curve of the ejector obtained by numerical simulations is compared with the experimental data reported in [9] in Fig. 3. By comparison, we also illustrate in the figure the results of the 2D simulations obtained by Mazzelli et al [9]. The predicted value of the entrainment ratio seems to be in good agreement with experimental data in on-design conditions. The numerical simulations tend, however, to overpredict the value of the critical back pressure, leading to significant discrepancies in off-design conditions. Finally, in terms of entrainment ratio, the numerical results obtained in the present study are very close to those reported in [9] all over the range of the back pressure.

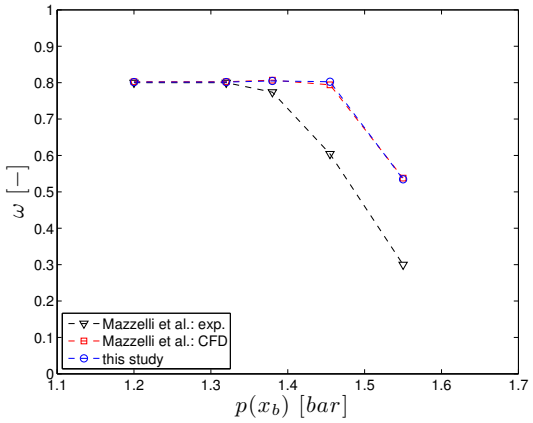

Figure 3. Comparison of the experimental characteristic curve of the ejector with numerical results.

We also assess the present numerical simulations against the flow topology observed in our experiments. For this purpose, the shock reflection pattern within the supersonic ejector was investigated through schlieren visualizations and compared to numerical schlieren (see Fig. 4). The latter was generated by computing the vertical gradient of the density field. As it can be observed in Fig. 4, numerical results are found to be in very good agreement with the experimental schlieren image. Note that for this schlieren image, the ejector operates in on-design conditions, and the flow structure is relatively stable at the exit of the primary nozzle. By contrast, in the off-design regime, the flow was found to be highly unstable, what makes a comparison of schlieren images with RANS simulations much less obvious. Once again, since the main purpose of this work consists in introducing new post-processing tools, the validation is limited to on-design conditions. The investigation of the flow structure within the ejector through schlieren visualizations in off-design conditions will be the subject of further publication.

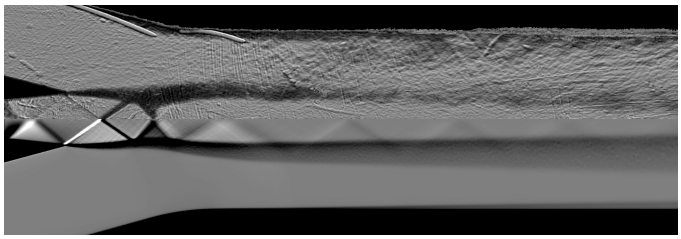

Figure 4. Comparison of experimental (top half) and numerical (bottom half) schlieren image (horizontal knife-edge) for $p(x_b) = 1.200\,[\text{bar}]$.

MOMENTUM AND ENERGY TUBES

In the study of Meyers and Meneveau [1], the authors introduced the concept of momentum and energy transport tubes as a transport visualization tool. These tubes are a generalization of the mass-flux based classical stream tubes. Just as there is, by construction, no average mass flux over the mantle of a stream tube, there will be on average no exchange of momentum or energy through a streamtube boundary, momentum and energy transport tubes will be constructed as surfaces with zero fluxes of the corresponding quantities. The construction of these tubes will therefore not be based on the velocity vector field, but rather by considering the vector fields formed by the total fluxes of momentum or energy. Since linear momentum is a vector quantity, it is proposed to define a direction characterized by a constant unit vector $\boldsymbol{\zeta}$ (and components ζ_i) and then to consider only the linear momentum in the $\boldsymbol{\zeta}$ direction, i.e. $\rho u_i \zeta_i$. The analysis developed by Meyers and Meneveau [1] for incompressible flows is here extended to compressible flows and in the absence of body forces. For statistically steady flows, the transport equation of the momentum in the $\boldsymbol{\zeta}$ direction is given by

$$\frac{\partial}{\partial x_j}\left(\underbrace{\hat{u}_j\overline{\rho}(\hat{u}_i\zeta_i) + \overline{\rho u_i'' u_j''}\zeta_i - \overline{\tau}_{ij}\zeta_i}_{\overline{F}_{m,j}}\right) = -\frac{\partial \overline{p}}{\partial x_i}\zeta_i \quad , \qquad (1)$$

where the ˆ stands for the Favre averaging and the $''$ symbol refers to the fluctuation compared to the Favre averaged quantity. The left-hand side of the equation is nothing else than the divergence of the vector field formed by the total flux of linear momentum in the $\boldsymbol{\zeta}$ direction, $\overline{\boldsymbol{F}}_m$, consisting of advective, turbulent and viscous fluxes, respectively. If we consider $\boldsymbol{\zeta} = \hat{\mathbf{e}}_x$, we will have for a 2D flow the following expression for the total flux of linear momentum

$$\overline{F}_{m,x} = \left(\hat{u}\overline{\rho}\hat{u} + \overline{\rho u'' u''} - \overline{\tau}_{xx}\right) \quad , \tag{2}$$

$$\overline{F}_{m,y} = \left(\hat{v}\overline{\rho}\hat{u} + \overline{\rho u'' v''} - \overline{\tau}_{xy}\right) \quad . \tag{3}$$

For the determination of energy tubes, a similar analysis is performed but in this case we investigate the transport equation for mean-flow kinetic energy $K = \overline{\rho}\hat{u}_i\hat{u}_i/2$,

$$\frac{\partial}{\partial x_j}\left(\overline{F}_{K,j}\right) = -\hat{u}_j\frac{\partial \overline{p}}{\partial x_j} - \overline{\tau}_{ij}\frac{\partial \hat{u}_i}{\partial x_j} + \overline{\rho u_i'' u_j''}\frac{\partial \hat{u}_i}{\partial x_j} \quad , \tag{4}$$

where $\overline{F}_{K,j}$ is the j^{th} component of the vector field formed by the total flux of kinetic energy, consisting of

$$\overline{F}_{K,j} = K\hat{u}_j + \overline{\rho u_i'' u_j''}\hat{u}_i - \overline{\tau}_{ij}\hat{u}_i \quad . \tag{5}$$

As it is pointed out in [1], such transport tubes are an interesting means of visualizing where the momentum and the energy in the flow are transported to, especially when transport processes are dominated by turbulence instead of mean-flow convection. Hence it may be very useful for the complex flow within a supersonic ejector.

RESULTS

Transport of mass, momentum and energy within the ejector

Fig. 5 shows the application of the concept of momentum and energy transport tubes to the ejector. First of all, for each set of operating conditions, the dividing streamline is shown (in *red*) on both halves in order to evaluate which part of the ejector is occupied by the primary stream. The dividing streamline is defined as the streamline passing through the point located in the nozzle exit plane at $y = h + \varepsilon$ with $\varepsilon \ll h$, i.e. just above the tip of the primary nozzle in order to avoid problems that would be caused by a potential separation of the flow within the primary nozzle.

Superimposed on these streamlines, a momentum (in *green*) and a kinetic energy (in *blue*) transport tubes are illustrated, in the top half of the ejector. For two-dimensional flows, a transport tube may be fully pictured by two transport lines. For the flow within the ejector, transport lines originating from two points located in the nozzle exit plane are considered sincetransport processes originate from that point. The first transport line starts

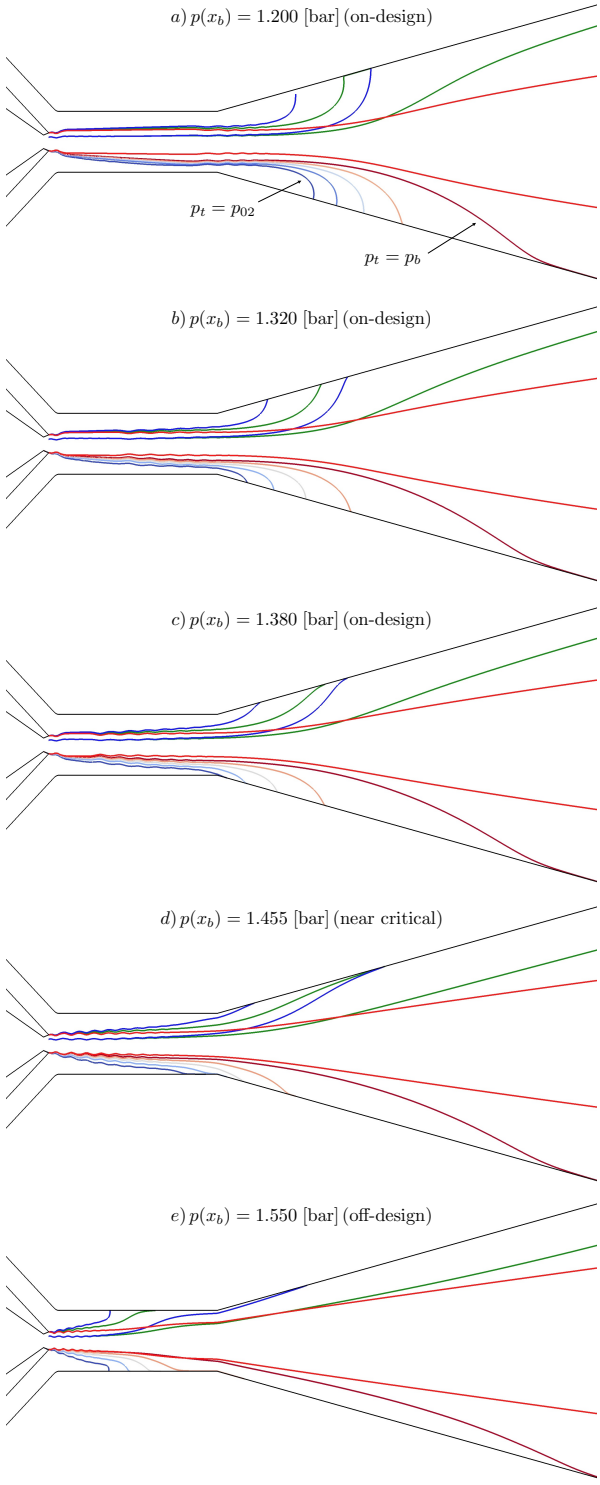

Figure 5. Momentum (*green*) and kinetic energy (*blue*) tubes (top half) and iso-contours of total pressure (bottom half) for different values of the back pressure. Note that the ejector is depicted with a fourfold stretching in the vertical direction for better visualization.

from $y = h/2$ while the other begins at $y = h + \varepsilon$, both for the momentum and the kinetic energy.

In order to illustrate the increase in total exergy (defined in eq. 11) of the secondary stream, iso-contours of total pressure are shown in the bottom half of the ejector. Indeed, it can be shown that for a perfect gas with constant specific heat capacities, the change in total exergy between two arbitrary states a and b is solely due to a change in total pressure

$$\Delta e_t = (e_{t,b} - e_{t,a}) = T_{\text{ref}} R^* \ln \frac{p_{t,b}}{p_{t,a}} \tag{6}$$

if total enthalpy is conserved through the process. Since in this study the total temperature is the same at both inlets and the flow is adiabatic within the ejector, iso-contours of total pressure are very close to iso-contours of exergy. Five iso-contours are shown here, equally distributed over the possible range of variation for the secondary stream, i.e. from $p_t = p_{02}$ to $p_t = p(x_b)$.

Two remarks may be made about the results shown in Fig. 5. Firstly, it appears that the momentum and kinetic energy transport lines originating from the tip of the primary nozzle are good indicators of the location where the exergy begins to increase in the core of the secondary stream. Secondly, the transport of momentum and kinetic energy from one stream towards the other takes place not only in the mixing duct, but also in the diffuser. This is especially true in on-design conditions: iso-contours of total pressure then indicate that a certain fraction of the secondary stream enters the diffuser with a total pressure lower than its reservoir condition, since the iso-contour $p_t = p_{02}$ reaches the wall in the diffuser. Hence, for low values of the back pressure, a substantial part of the exergy transfer occurs in the diffuser. It should be noted that this is not in agreement with 1D approximations which state that both streams are already completely mixed well within the mixing duct [2, 3].

New indicators of mixing

For the investigation of the transfer phenomena within the ejector, the dimensionless cumulative transfer of momentum between the primary and the secondary stream, $I_m(x)$, is introduced

$$I_m(x) = \frac{\int\int_{S(x)} \overline{\boldsymbol{F}}_m \cdot \mathbf{ds}}{\dot{m}_1 U_1} \quad , \tag{7}$$

where $S(x)$ is defined as the portion of the dividing surface between the nozzle exit plane, x_{xnp}, and x. Obviously, for 2D-flows, the dividing surface simply consists in the extrusion of the dividing streamline. The flux is considered as positive when it leaves the primary stream to enter the secondary stream. Note that the speed U_1 is defined as $U_1 = \sqrt{2h_{01}}$ and corresponds to the maximum speed that the primary stream could reach through an adiabatic flow without any shaft work (i.e. a flow for which total enthalpy would be conserved). The corresponding quantity for the mean-flow kinetic energy is given by

$$I_K(x) = \frac{\int\int_{S(x)} \overline{\boldsymbol{F}}_K \cdot \mathbf{ds}}{\dot{m}_1 h_{01}} \quad . \tag{8}$$

The profile of $I_m(x)$ is shown in Fig. 6 for different operating conditions. Note that the profile of $I_K(x)$ was very similar to $I_m(x)$ so it is not shown here. The results confirm the different remarks made in the previous subsection. It should be noted that when the ejector is operating in the on-design regime, the slope of the cumulative flux of linear momentum crossing the dividing surface is larger in the diffuser than in the mixing duct. This means that the momentum transfer is actually more important in the diffuser than in the mixing duct. Here again, it seems that numerical results show significant discrepancies with 1D models which predict full mixing before the entry of the diffuser [2, 3]. In addition, as it could be seen with the momentum and kinetic energy tubes, it appears that, in off-design operations, the transfer of momentum takes place almost entirely in the mixing duct.

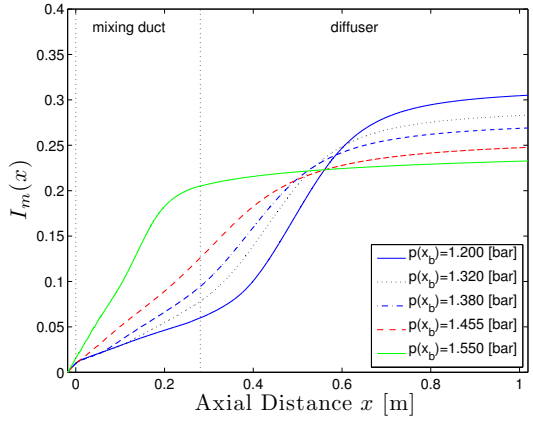

Figure 6. Cumulative flux of linear momentum (in the horizontal direction) crossing the dividing streamline for different values of the back pressure.

Moreover, it can also be observed in Fig. 6 that the global momentum transfer increases when the back pressure decreases. The following analysis will show that it does not necessarily mean that the mixing is more efficient.

The dimensionless gain in exergy of the secondary stream between the primary nozzle exit position and x, $\xi(x)$, is defined as

$$\xi(x) = \frac{\dot{m}_2 \left(e_{t_2}(x) - e_{t_2}(x_{\text{nxp}})\right)}{\dot{m}_1 e_{01}} \quad , \tag{9}$$

where $e_{t_2}(x)$ is the mass flow-averaged total exergy flux associated with the secondary stream, i.e.

$$e_{t_2}(x) = \frac{\int\int_{A_2(x)} \overline{\rho} e_t \hat{\mathbf{u}} \cdot \mathbf{ds}}{\dot{m}_2} \quad , \tag{10}$$

with $A_2(x)$ the section through which the secondary stream flows and e_t the specific total exergy defined by

$$e_t = (h_t - h_{\text{ref}}) - T_{\text{ref}}\,(s - s_{\text{ref}}) \quad , \tag{11}$$

where the subscript "ref" refers to the reference state (or *dead* state), generally defined by $T_{\text{ref}} = 300\,[\text{K}]$ and $p_{\text{ref}} = 1\,[\text{bar}]$. Note that the stagnation value of the enthalpy is considered in this definition to account for the exergetic content of the kinetic energy, which is often omitted.

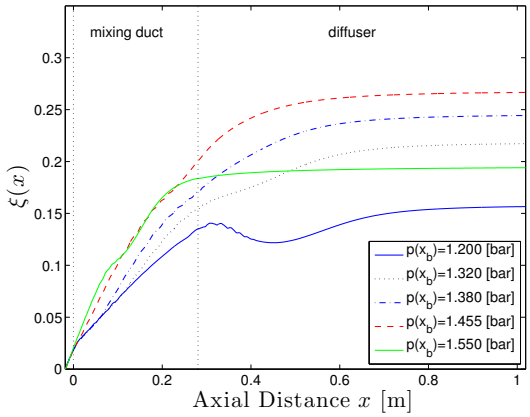

Figure 7. Gain in exergy of the secondary stream for different values of the back pressure.

Results are shown in Fig. 7 for different operating conditions. It appears clearly that, unless the ejector is run at a off-design regime, the exergy transfer is not complete at the entry of the diffuser. This fact confirms that a certain part of the mixing between both streams takes place in the diffuser. However, it should be noted that the exergy analysis reveals additional information about the quality of the mixing. For very low values of the back pressure, the flux of total exergy associated with the secondary stream may decrease due to important shock waves. Indeed, the latter inevitably generate an increase of entropy and therefore a decrease of exergy in the flow. Moreover, it appears that the gain in exergy of the secondary stream is maximum for a value of the back pressure close to the critical pressure ($p(x_b) = 1.455\,[\text{bar}]$), although the global transfer of momentum is not maximum in this situation.

CONCLUSION

The present study has applied the momentum and energy tube analysis tools of [1] to investigate the key transport phenomena occuring along a supersonic ejector. Used jointly with new indicators of mixing, it brings insights into the locations where the transfers of exergy and momentum occur. These indicators are based on the cumulative transfer of linear momentum between both streams and the gain in exergy of the secondary stream. It is shown that transfers still occur in the diffuser, in particular in on-design conditions, contrary to the usual assumptions of 1D models. Although the global transfer of momentum increases when the back pressure decreases, the gain in exergy of the secondary stream is maximum for a value of the back pressure close to the critical one.

REFERENCES

[1] Johan Meyers and Charles Meneveau. Flow visualization using momentum and energy transport tubes and applications to turbulent flow in wind farms. *Journal of Fluid Mechanics*, 715:335–358, 2013.

[2] B.J. Huang, J.M. Chang, C.P. Wang, and V.A. Petrenko. A 1-d analysis of ejector performance. *International Journal of Refrigeration*, 22(5):354 – 364, 1999.

[3] Fanshi Kong and H.D. Kim. Analytical and computational studies on the performance of a two-stage ejectordiffuser system. *International Journal of Heat and Mass Transfer*, 85:71 – 87, 2015.

[4] T. Sriveerakul, S. Aphornratana, and K. Chunnanond. Performance prediction of steam ejector using computational fluid dynamics: Part 2. flow structure of a steam ejector influenced by operating pressures and geometries. *International Journal of Thermal Sciences*, 46(8):823 – 833, 2007.

[5] A. Hemidi, F. Henry, S. Leclaire, J.-M. Seynhaeve, and Y. Bartosiewicz. CFD analysis of a supersonic air ejector. part ii: Relation between global operation and local flow features. *Applied Thermal Engineering*, 29(1415):2990 – 2998, 2009.

[6] S. Croquer, S. Poncet, and Z. Aidoun. Turbulence modeling of a single-phase R134a supersonic ejector. part 2: Local flow structure and exergy analysis. *International Journal of Refrigeration*, 61:153 – 165, 2016.

[7] A. Kurganov, S. Noelle, and G. Petrova. Semidiscrete central-upwind schemes for hyperbolic conservation laws and hamilton–jacobi equations. *SIAM J. Sci. Comput.*, 23(3):707–740, March 2001.

[8] Christopher J. Greenshields, Henry G. Weller, Luca Gasparini, and Jason M. Reese. Implementation of semi-discrete, non-staggered central schemes in a colocated, polyhedral, finite volume framework, for high-speed viscous flows. *International Journal for Numerical Methods in Fluids*, 63:1–21, 2010.

[9] F. Mazzelli, A. B. Little, S. Garimella, and Y. Bartosiewicz. Computational and experimental analysis of supersonic air ejector: Turbulence modeling and assessment of 3d effects. *International Journal of Heat and Fluid Flow*, 56:305 – 316, 2015.

[10] C. Geuzaine and J.-F. Remacle. Gmsh: A 3-d finite element mesh generator with built-in pre-and post-processing facilities. *International Journal for Numerical Methods in Engineering*, 79(11):1309–1331, 2009.